Electronic Supplementary Information (ESI)

Optical enhancement of the highly-efficient organic-inorganic oxyfluoride red phosphor via cation co-doping strategy

Xiaoyi Liu[a,b], Haiming Cheng[c], Hu Wang[b], Zhu Wen[b], Guixia Liu*[a,b], Shengda Liu[b], Dan Li[b], Jinxian Wang[b], Wensheng Yu[b], Xiangting Dong[b]

[a]*College of Materials Science and Engineering, Changchun University of Science and Technology, Changchun 130022, China*

[b]*Key Laboratory of Applied Chemistry and Nanotechnology at Universities of Jilin Province, Changchun University of Science and Technology, Changchun 130022, China*

[c]*State Key Laboratory of Inorganic Synthesis and Preparative Chemistry, College of Chemistry Jilin University, Changchun 130012, China.*

**Corresponding Author.*

Tel.: +86-431-85582574. Fax: +86-431-85383815

E-mail address: liuguixia22@163.com

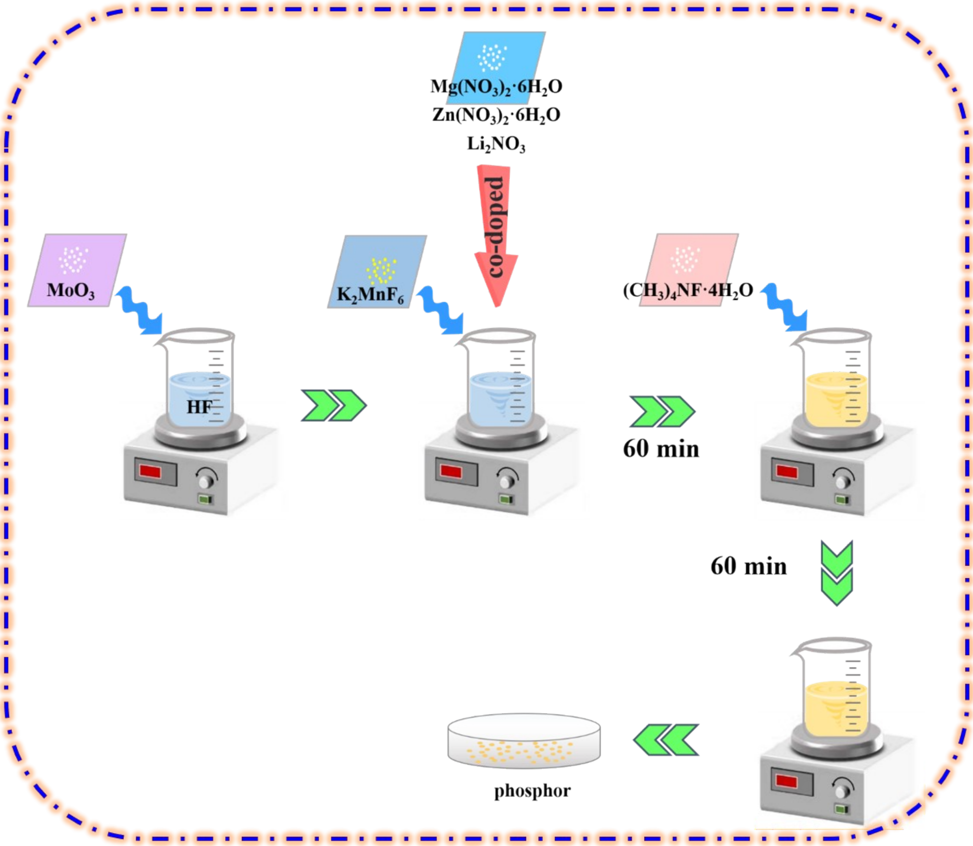

Fig. S1 Schematic diagram of the synthesis process of $[N(CH_3)_4]_3MoO_3F_3:Mn^{4+}$, $[N(CH_3)_4]_3MoO_3F_3:Mn^{4+}$, Mg^{2+}, $[N(CH_3)_4]_3MoO_3F_3:Mn^{4+}$, Zn^{2+} and $[N(CH_3)_4]_3MoO_3F_3:Mn^{4+}$, Li^{+}, The special $3d^3$ valence electronic structure of Mn^{4+} could be well-described by the Tanabe-Sugano energy level diagram, which is shown in **Fig. S2a**. In order to better understand the photoluminescence mechanism of $[N(CH_3)_4]_3MoO_3F_3:Mn^{4+}$ phosphor, the corresponding crystal field strength (D_q) and Racah parameters (B, C) for Mn^{4+} occupied the octahedral site were calculated according to the equations (1) - (4) listed as follows **[24, 37]**:

$$E(^4T_{2g} \rightarrow {}^4A_{2g}) = 10D_q \qquad (1)$$

$$\frac{B}{D_q} = \frac{\left(\frac{\Delta E}{D_q}\right)^2 - 10\left(\frac{\Delta E}{D_q}\right)}{15\left(\frac{\Delta E}{D_q} - 8\right)} \qquad (2)$$

$$\Delta E = E(^4T_{1g}) - E(^4T_{2g}) \qquad (3)$$

$$\frac{E(^2E_g)}{B} = \frac{3.05C}{B} + 7.90 - \frac{1.80B}{D_q} \qquad (4)$$

In our work, the ZPL energy of the ^2E_g state can be determined easily to be 16051 cm^{-1} (624 nm) from the experimental PL spectrum. However, when determining the $^4T_{2g}$ and $^4T_{1g}$ energy levels, their strong phonon coupling needs to be considered, because their equilibrium energy levels are not simply given by the peak energy of each PLE band, but by the ZPL energy. For the convenience of calculation, $E(^4A_{2g} \rightarrow {}^4T_{1g})$ and $E(^4A_{2g} \rightarrow {}^4T_{2g})$ are identified as 27027 cm^{-1} (370 nm) and 21277 cm^{-1} (470 nm) according to the strongest peaks of the absorption spectrum, respectively. Subsequently, crystal field intensity (D_q =2128 cm^{-1}), Racah parameters (B = 528 cm^{-1} and C = 3964 cm^{-1}) were calculated, which believes that the $[N(CH_3)_4]_3MoO_3F_3$ matrix provides a strong crystal field environment (D_q/B = 4.03) for Mn^{4+}.

Proverbially, the energy level difference of $^2E_g \rightarrow {}^4A_{2g}$ has little relation with the crystal field intensity D_q, which is mainly determined by nephelauxetic effect. Moreover, the reduction degree of Racah parameters B and C parameters varies with different matrix. Therefore, β_1 can be calculated according to equation (5) and used to quantitatively describe nephelauxetic effect in Mn^{4+} ion spectra **[24]**:

$$\beta_1 = \sqrt{\left(\frac{B}{B_0}\right)^2 + \left(\frac{C}{C_0}\right)^2} \qquad (5)$$

Herein, B_0 = 1160 cm^{-1}, C_0 = 4303 cm^{-1}, so the β_1 value of Mn^{4+} in $[N(CH_3)_4]_3MoO_3F_3$ matrix is calculated to be 1.03. According to the data between β_1 value and emission peak energy $E(^2E_g \rightarrow ^4A_{2g})$ in different matrix materials of Mn^{4+} (**Table S1**) **[23-36]**, the ^2E_g level energy can be expressed as a linear function of β_1, $E(^2E_g) = 18111.57\beta_1 - 2596.03$ (**Fig. S2b**). When $\beta_1 = 1.03$, $E(^2E_g)$ = 16059 cm^{-1}, which is close to the experimental value (16026 cm^{-1}), this linear function can predict the energy position of ^2E_g. Meanwhile, the emission peak energy of Mn^{4+} is close to the reported $^2E_g \rightarrow ^4A_{2g}$ emission peak energies of Mn^{4+} in fluoride and oxyfluoride, which demonstrates that the nephelauxetic effect of Mn^{4+} ions in the $[N(CH_3)_4]_3MoO_3F_3$ matrix is weaker than that in the oxide matrix.

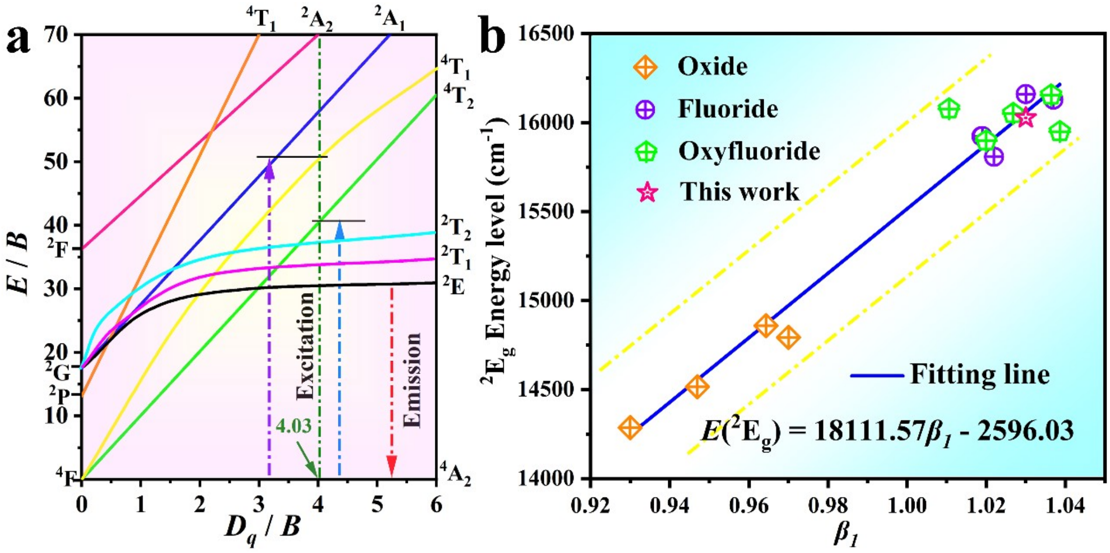

Fig. S2 Tanabe-Sugano energy-level diagram of Mn^{4+} in $[N(CH_3)_4]_3MoO_3F_3$ host (a), and the relationship (b) between $E(^2E_g \rightarrow ^4A_{2g})$ and β_1 of Mn^{4+} in different hosts

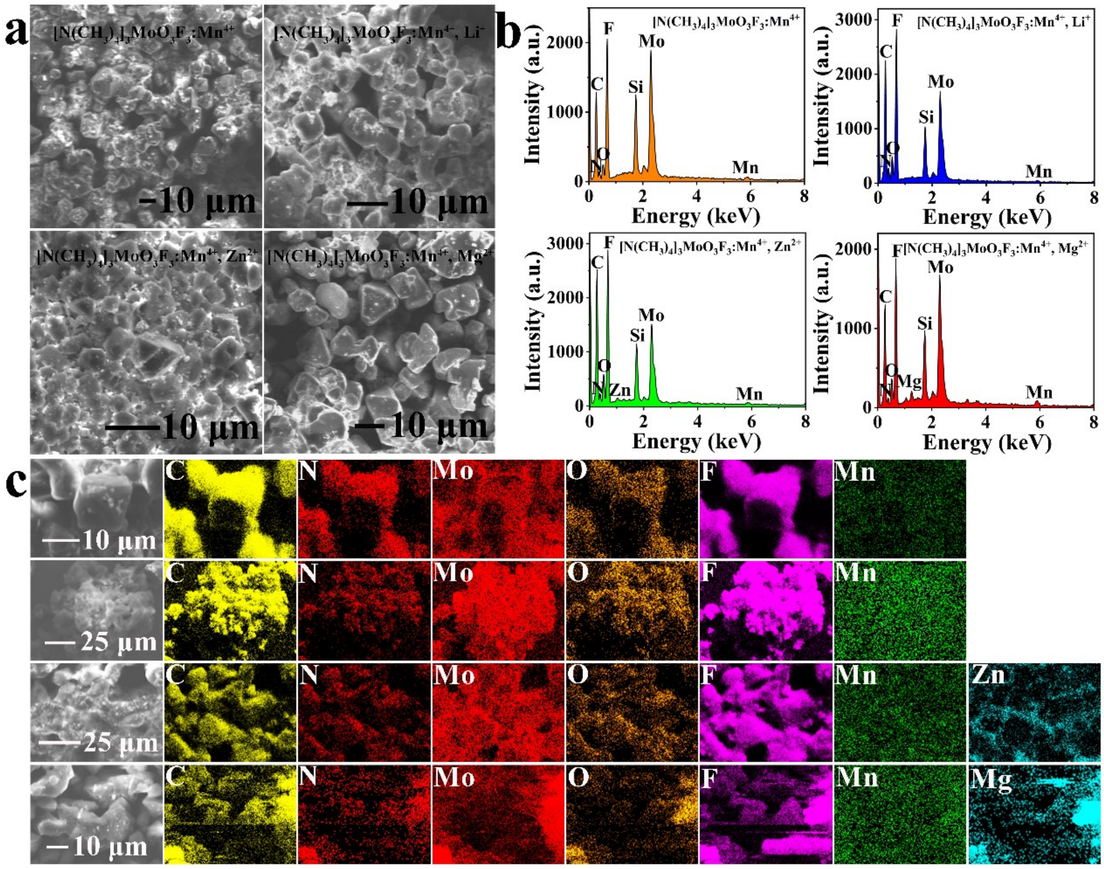

Fig. S3 SEM images (a) EDS spectra (b) and elemental mapping images (c) of $[N(CH_3)_4]_3MoO_3F_3$ synthesized by co-doping different cations

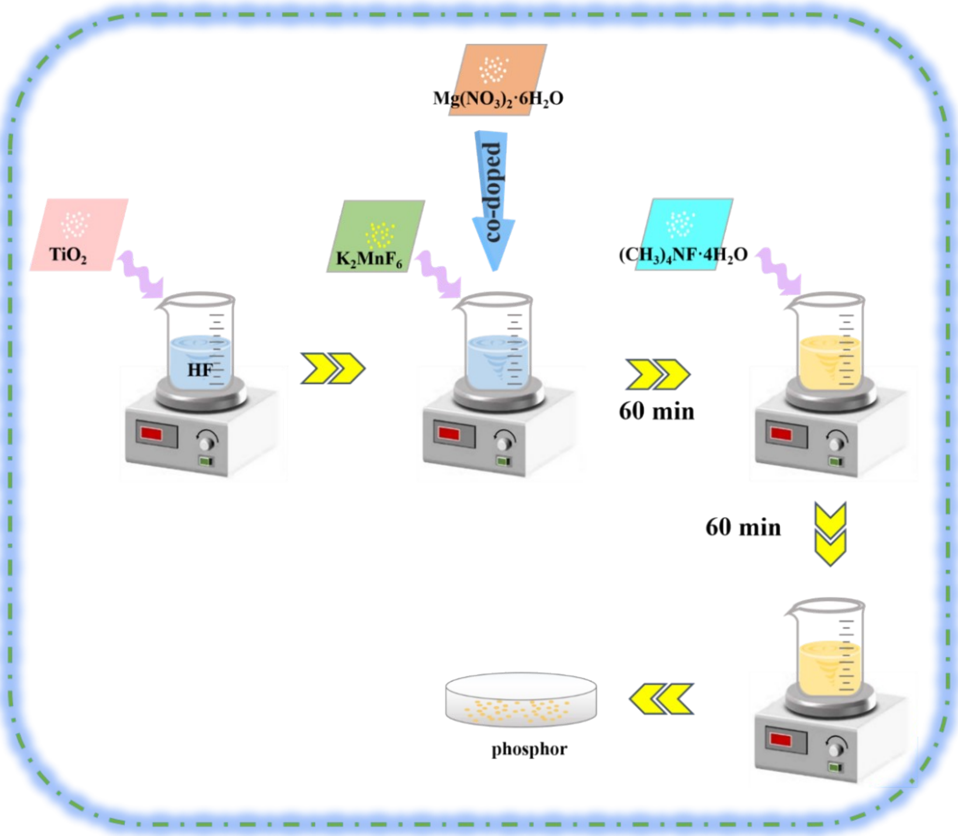

Fig. S4 Schematic diagram of the synthesis process of $[N(CH_3)_4]_2TiF_6{:}Mn^{4+}$, $[N(CH_3)_4]_2TiF_6{:}Mn^{4+}$, Mg^{2+}

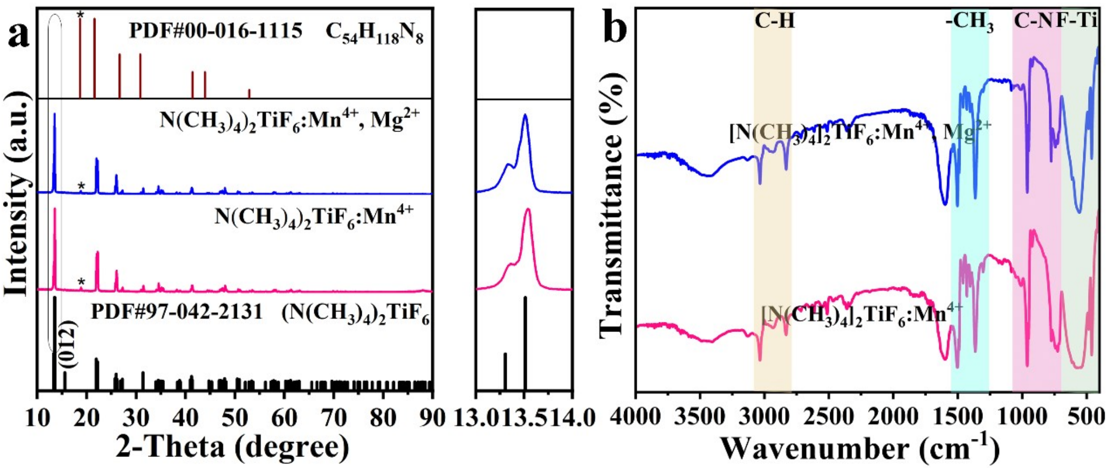

Fig. S5 XRD patterns (a) FT-IR spectra (b) of $[N(CH_3)_4]_2TiF_6:Mn^{4+}$ and $[N(CH_3)_4]_2TiF_6:Mn^{4+}$, Mg^{2+}

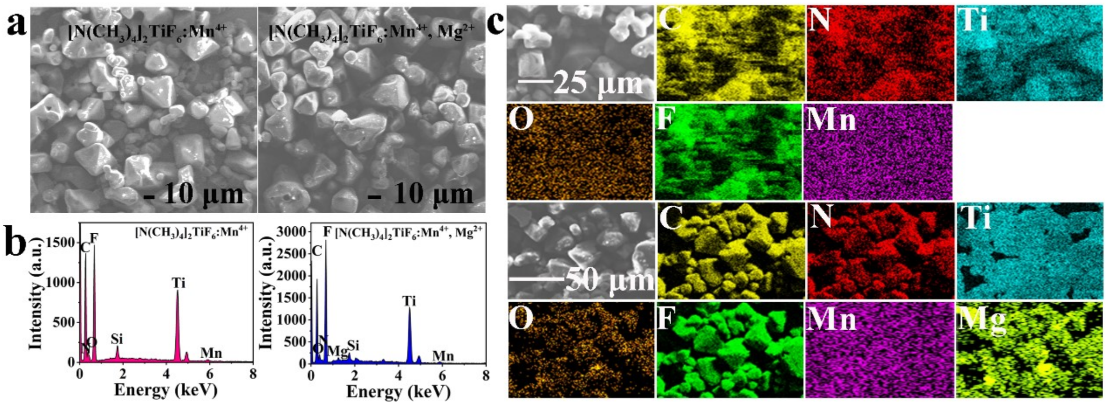

Fig. S6 SEM images (a), EDS spectra (b) and elemental mapping images (c) of $[N(CH_3)_4]_2TiF_6:Mn^{4+}$ and $[N(CH_3)_4]_2TiF_6:Mn^{4+}, Mg^{2+}$

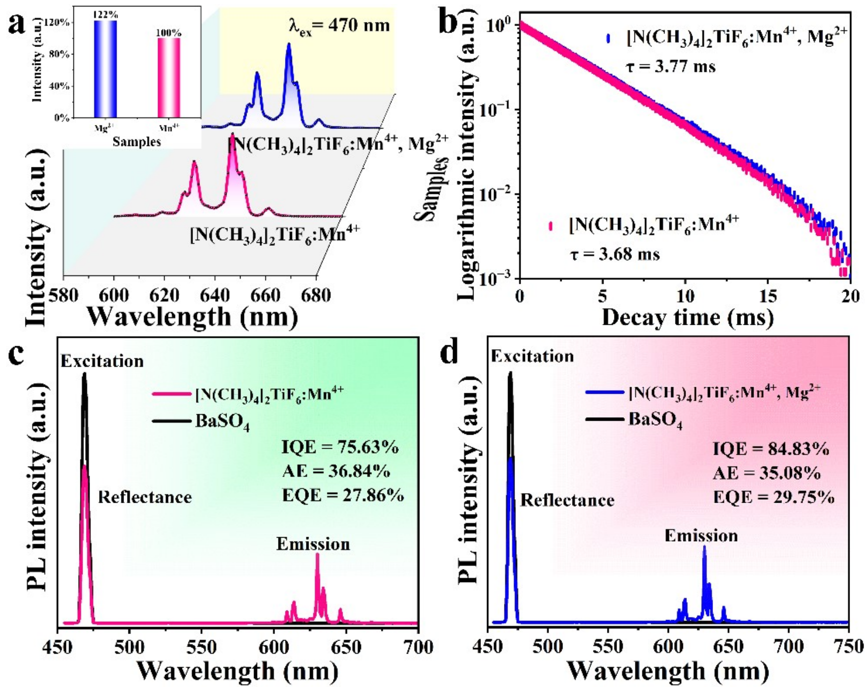

Fig. S7 Emission spectra and emission intensity histogram (a), decay curves (b), and spectra (c and d) of $[N(CH_3)_4]_2TiF_6:Mn^{4+}$ and $[N(CH_3)_4]_2TiF_6:Mn^{4+}$, Mg^{2+} and the reference sample measured using an integrating sphere for IQE, AE and EQE

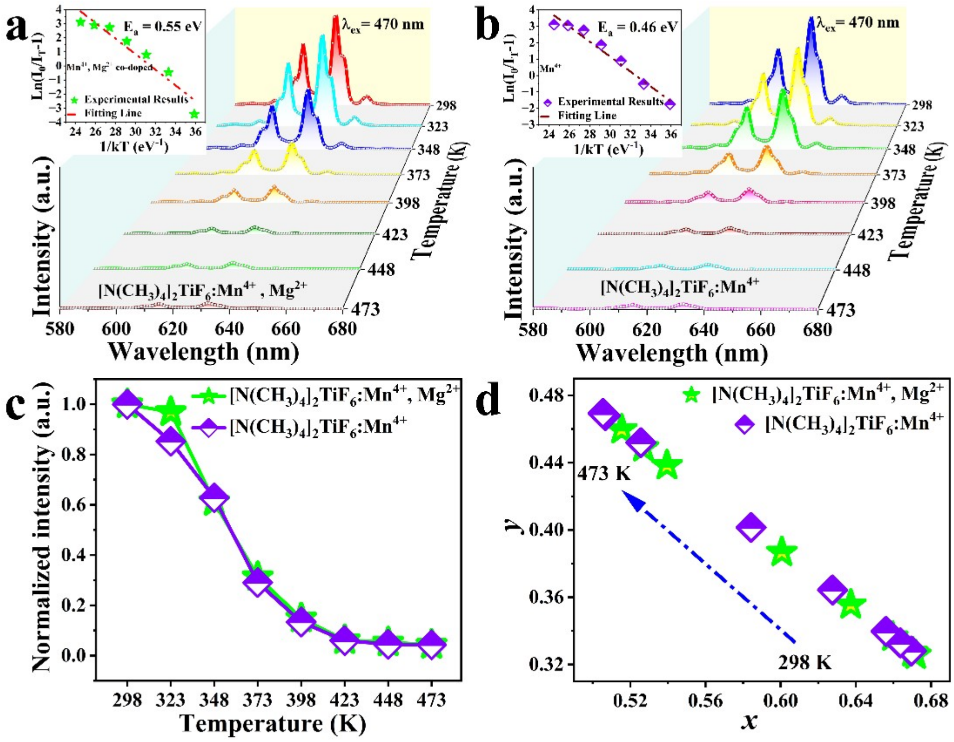

Fig. S8 Temperature-dependent PL spectra and Arrhenius fitting for different phosphors to deduce the activation energy (E_a) (a and b), relative intensity (c) and CIE coordinates at different temperature (d) of $[N(CH_3)_4]_2TiF_6:Mn^{4+}$ and $[N(CH_3)_4]_2TiF_6:Mn^{4+}, Mg^{2+}$

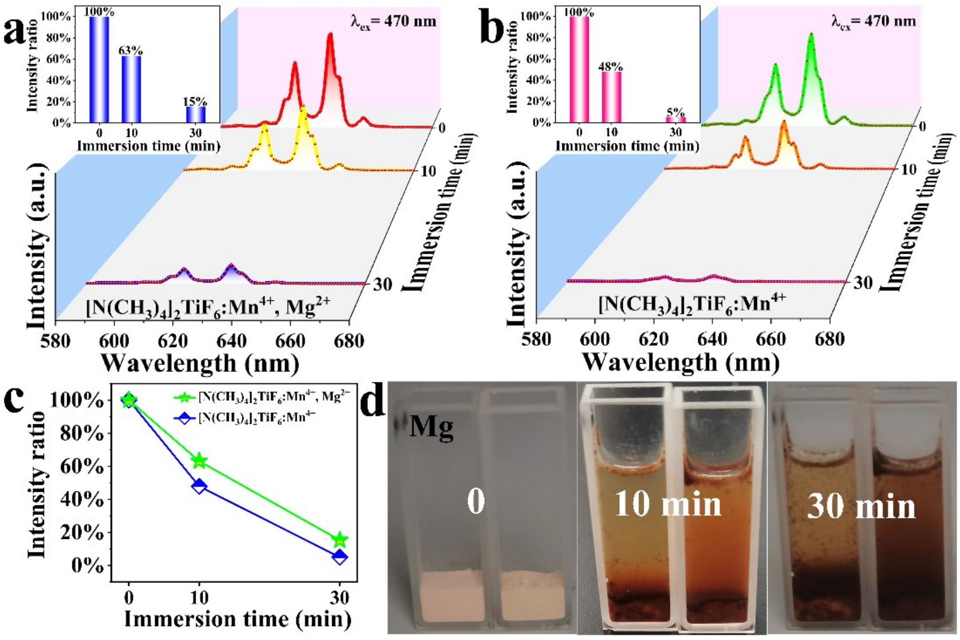

Fig. S9 Corresponding emission spectra and emission intensity histogram (a and b) of $[N(CH_3)_4]_2TiF_6:Mn^{4+}$ and $[N(CH_3)_4]_2TiF_6:Mn^{4+}$,Mg^{2+} for different immersion times (0, 10 min and 30 min) in deionized water, the changes (c) of PL intensity ratio of these red phosphors at 632 nm with different immersion time and photographs (d) of exposed to natural light

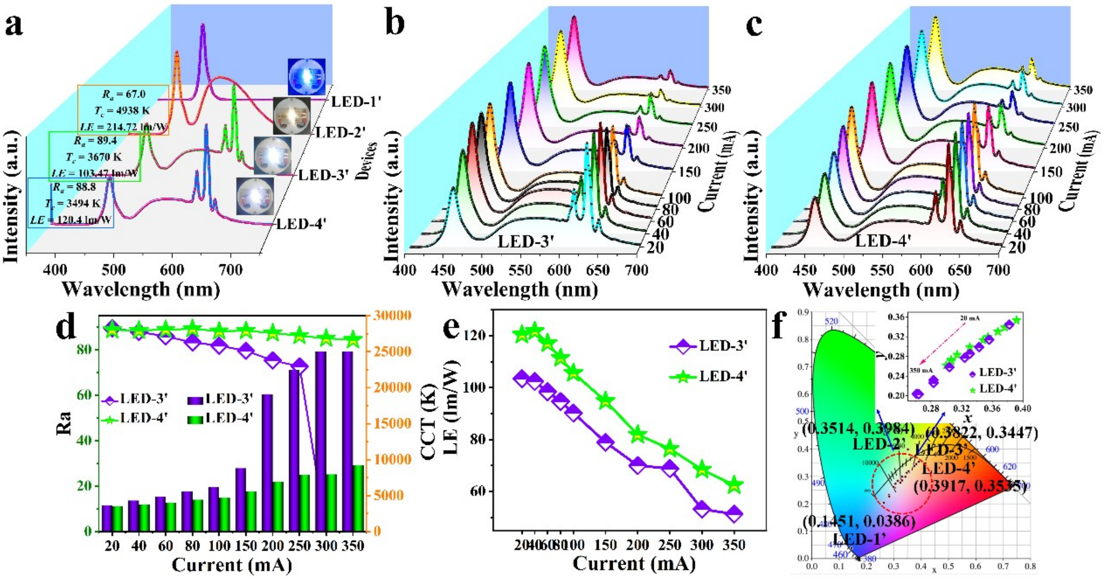

Fig. S10 Electroluminescence (EL) spectra of LED devices (a), EL spectra (b and c), the changes of CRI and CCT (d), LE (e) and CIE color coordinates (f) under different driving currents (20-350 mA) of the LED-3' and LED-4'

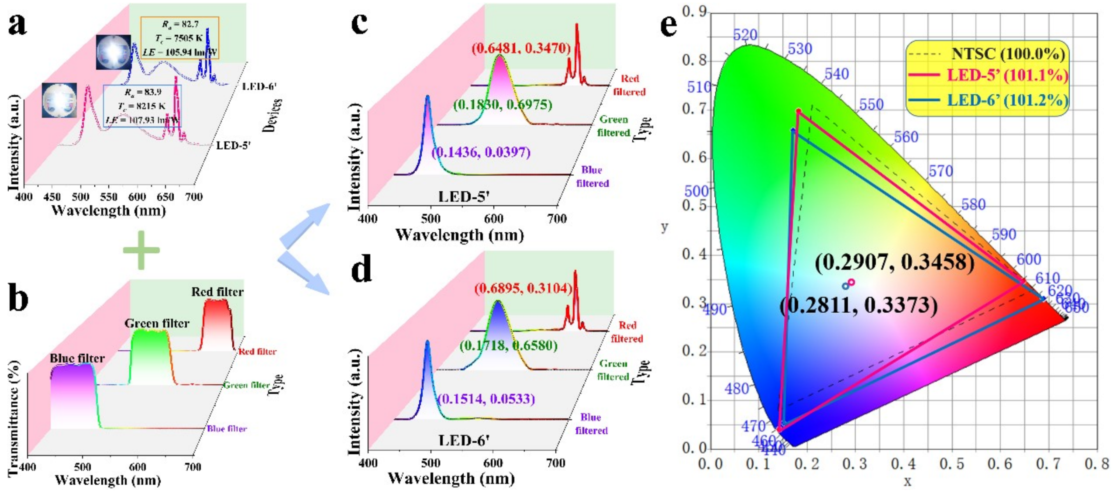

Fig. S11 EL spectrum (a), transmittance spectra (b) of the commercial blue, green, and red color filters, the corresponding blue, green and red EL spectra after filtering (c and d) and CIE color coordinates (e) of the WLED and the NTSC standard in the CIE 1931 color space

Table S1. Schemes of different molecular ratios of chemical reagent for the synthesis of red phosphors

samples	$MoO_3 : K_2MnF_6$ (Molar ratio %)	MoO_3 : $Mg(NO_3)_2{\cdot}6H_2O/Zn(NO_3)_2{\cdot}6H_2O/LiNO_3$ (Molar ratio %)
2%Mn^{4+}	98 : 2	
4%Mn^{4+}	96 : 4	
6%Mn^{4+}	94 : 6	
8%Mn^{4+}	92 : 8	
10%Mn^{4+}	90 : 10	
6%Mn^{4+}, 10%Mg^{2+}	84 : 6	84 : 10
6%Mn^{4+}, 10%Zn^{2+}	84 : 6	84 : 10
6%Mn^{4+}, 10%Li^{+}	84 : 6	84 : 10

Table S2 Spectroscopic parameters and β_1 values of Mn^{4+} ions for as-reported Mn^{4+}-activated fluorides, oxyfluorides and oxides phosphor.

Host	D_q/cm^{-1}	B/cm^{-1}	D_q/B	C/cm^{-1}	β_1/cm^{-1}	$E(^2E_g)$ /cm^{-1}	Ref.
$Li_3Na_3Ga_2F_{12}$	2146	548	3.9	3884	1.02	15923	[23]
Cs_2NaGaF_6:Mn^{4+}	2137	526	4.1	3923	1.02	15808	[24]
K_2XF_7(X=Ta, Nb)	2166	551	3.9	3955	1.03	16160	[25]
Na_2TiF_6	2100	505	4.2	4052.6	1.04	16129	[26]
$Na_3Li_3In_2F_{12}$:Mn^{4+}	2137	549	3.9	3881	1.02	15924	[27]
$Na_2WO_2F_4$	2132	546	3.9	3973	1.04	16155	[28]
$K_2[MoO_2F_4]\cdot H_2O$	2123	510	4.2	4049	1.04	15949	[29]
$Rb_2MoO_2F_4$	2137	557	3.8	3905	1.03	16051	[30]
$K_3WO_2F_5\cdot 2H_2O$	2128	489	4.4	4061	1.03	16051	[31]
$BaNbF_{5.5}(OH)_{1.5}$	2128	505	4.2	3975	1.02	15898	[32]
Li_4AlSbO_6	2146	745	2.9	3095	0.96	14859	[33]
$BaLaLiTe_{1-x}O_6$	2123	734	2.9	2932	0.93	14286	[34]
Ba_2CaWO_6	2024	788	2.6	2989	0.97	14793	[35]
Ba_2LaNbO_6	1965	688	2.1	3175	0.947	14684	[36]

Table S3 Cell parameters of $[N(CH_3)_4]_3MoO_3F_3$, $[N(CH_3)_4]_3MoO_3F_3$:Mn^{4+}, $[N(CH_3)_4]_3MoO_3F_3$:Mn^{4+}, Mg^{2+}, $[N(CH_3)_4]_3MoO_3F_3$:Mn^{4+}, Zn^{2+} and $[N(CH_3)_4]_3MoO_3F_3$:Mn^{4+}, Li^{+} phosphors

Samples	**Crystalline phase**	**Space group**	**Lattice parameters**	
			a=b=c(Å)	**V(Å^3)**
host	Cubic	*Pa*-3(205)	14.1565	2837.10
Mn^{4+}	Cubic	*Pa*-3(205)	14.1348	2824.05
Mn^{4+}, Mg^{2+}	cubic	*Pa*-3(205)	14.1772	2849.54
Mn^{4+}, Zn^{2+}	cubic	*Pa*-3(205)	14.1667	2843.19
Mn^{4+}, Li^{+}	cubic	*Pa*-3(205)	14.1494	2832.81

Table S4 Cell parameters of $[N(CH_3)_4]_2TiF_6$, $[N(CH_3)_4]_2TiF_6:Mn^{4+}$ and $[N(CH_3)_4]_2TiF_6:Mn^{4+}, Mg^{2+}$ phosphors

Samples	**Crystalline phase**	**Space group**	**Lattice parameters**	
			a=b=c(Å)	**V(Å^3)**
host	hexagonal	*R*-3(148)	8.004	1106.80
Mn^{4+}	hexagonal	*R*-3(148)	7.991	1099.81
Mn^{4+}, Mg^{2+}	hexagonal	*R*-3(148)	8.004	1107.02

Table S5 Important photoelectric parameters of the LED devices under different driving currents (20-350 mA).

Device	Current (mA)	R_a	T_c (K)	CIE (x,y)	R_9	Luminous efficiency (lm/W)
LED-1	20	0	25000	(0.1462, 0.0338)	-286	34.99
LED-2	20	64.7	4610	(0.3671, 0.4246)	-69	225.62
LED-3	20	89.0	3224	(0.4080, 0.3665)	75	88.41
	40	88.1	3504	(0.3915, 0.3540)	69	83.42
	60	87.3	3728	(0.3799, 0.3433)	68	79.28
	80	86.3	3834	(0.3754, 0.3399)	64	73.78
	100	85.6	4030	(0.3672, 0.3314)	63	68.49
	150	85.1	4322	(0.3570, 0.3190)	65	58.31
	200	84.9	4428	(0.3536, 0.3146)	66	49.06
	250	94.5	4558	(0.3503, 0.3112)	65	40.81
	300	85.5	5695	(0.3293, 0.2833)	90	33.54
	350	80.5	8570	(0.3077, 0.2536)	48	22.17
LED-4	20	87.7	3520	(0.4045, 0.3910)	60	125.89
	40	85.4	3632	(0.3987, 0.3886)	50	123.27
	60	84.0	3710	(0.3948, 0.3869)	44	118.63
	80	83.1	3766	(0.3920, 0.3856)	39	114.31
	100	81.6	3834	(0.3888, 0.3837)	34	109.07
	150	80.0	3964	(0.3822, 0.3784)	25	97.39
	200	78.9	4052	(0.3779, 0.3742)	20	88.54
	250	77.5	4214	(0.3706, 0.3673)	14	80.37
	300	77.8	4226	(0.3696, 0.3644)	16	72.19
	350	80.2	4572	(0.3549, 0.3413)	27	58.59
LED-5	20	81.4	6845	(0.2965, 0.3367)	24	80.47
LED-6	20	82.2	7310	(0.3039, 0.3427)	18	78.86

Table S6 Important photoelectric parameters of the LED devices under different driving currents (20-350 mA).

Device	Current (mA)	R_a	T_c (K)	CIE (x,y)	R_9	Luminous efficiency (lm/W)
LED-1’	20	0	25000	(0.1451, 0.0386)	-254	34.16
LED-2’	20	67.0	4938	(0.3514, 0.3984)	-58	214.72
LED-3’	20	89.4	3670	(0.3822, 0.3447)	90	103.47
	40	87.9	4320	(0.3560, 0.3141)	70	102.44
	60	85.9	4856	(0.3429, 0.2992)	59	98.42
	80	83.3	5585	(0.3307, 0.2855)	45	94.69
	100	81.8	6145	(0.3240, 0.2773)	36	90.25
	150	79.6	8810	(0.3041, 0.2584)	30	78.94
	200	75.3	19060	(0.2833, 0.2320)	9	69.99
	250	72.7	22500	(0.2834, 0.2264)	-13	68.86
	300	0	25000	(0.2615, 0.2039)	5	53.15
	350	0	25000	(0.2641, 0.2034)	-11	51.30
LED-4’	20	88.8	3494	(0.3917, 0.3535)	87	120.40
	40	88.5	3794	(0.3764, 0.3391)	85	121.74
	60	88.9	4022	(0.3673, 0.3305)	85	117.11
	80	89.2	4436	(0.3544, 0.3193)	85	111.42
	100	88.2	4678	(0.3481, 0.3132)	85	105.66
	150	88.4	5590	(0.3307, 0.2989)	89	94.84
	200	87.4	6905	(0.3142, 0.2834)	88	81.86
	250	86.2	7905	(0.3063, 0.2730)	83	76.45
	300	85.0	7955	(0.3067, 0.2704)	74	68.40
	350	84.4	9175	(0.3000, 0.2618)	69	62.39
LED-5’	20	83.9	8215	(0.2907, 0.3458)	44	107.93
LED-6’	20	82.7	7505	(0.2811, 0.3373)	32	105.94